HHS Public Access

Author manuscript

Alcohol (Hanover). Author manuscript; available in PMC 2024 February 01.

Published in final edited form as:

Alcohol (Hanover). 2023 February ; 47(2): 219–239. doi:10.1111/acer.15000.

Repeated ethanol exposure and withdrawal alters angiotensin-converting enzyme 2 expression in discrete brain regions: Implications for SARS-CoV-2 neuroinvasion

Nagalakshmi Balasubramanian, PhD,

Thomas D James, PhD,

Govindhasamy Pushpavathi Selvakumar, PhD,

Jessica Reinhardt, MSc,

Catherine A. Marcinkiewcz, PhD

Department of Neuroscience and Pharmacology, University of Iowa, Iowa City, IA-52242, USA

Abstract

Background: People with alcohol use disorders (AUD) may be at higher risk for COVID-19. Angiotensin-converting enzyme 2 (ACE2) and transmembrane serine protease 2 (TMPRSS2) are required for cellular entry of SARS-CoV-2, but information on their expression in specific brain regions after alcohol exposure is limited. We sought to clarify how chronic alcohol exposure affects ACE2 expression in monoaminergic brainstem circuits and other putative SARS-CoV-2 entry points.

Methods: Brains were examined for ACE2 using immunofluorescence after 4 weeks of chronic intermittent ethanol (CIE) vapor inhalation. Additionally, we examined TMPRSS2, Cathepsin L, and ADAM17 by Western blot and RAS pathway mediators and pro-inflammatory markers via RT-qPCR.

Results: ACE2 increased in most brain regions following CIE including olfactory bulb (OB), hypothalamus (HT), raphe magnus (RMG), raphe obscurus (ROB), locus coeruleus (LC), and periaqueductal gray (PAG). We also observed increased colocalization of ACE2 with monoaminergic neurons in brainstem nuclei. Moreover, soluble ACE2 (sACE2) was elevated in OB, HT, and LC. This increase in sACE2 in OB and HT was accompanied by upregulation of ADAM17, an ACE2 sheddase, while TMPRSS2 increased in HT and LC. Cathepsin L, an endosomal receptor involved in viral entry, was also increased in OB. Alcohol can increase Angiotensin II, which triggers a pro-inflammatory response that may upregulate ACE2 via activation of RAS pathway receptors AT1R/AT2R. ACE2 then metabolizes Angiotensin II to Angiotensin (1-7) and provokes an anti-inflammatory response via MAS1. Accordingly, we report that AT1R/AT2R mRNA decreased in OB and increased in the LC, while MAS1 mRNA increased

Please send all correspondence to: Catherine A. Marcinkiewcz, Department of Neuroscience and Pharmacology, University of Iowa, Iowa City, IA-52242, USA, catherine-marcinkiewcz@uiowa.edu, Fax: 319-335-8930, Phone: 319-335-6944.

Disclosure

The authors declare that they have no conflict of interest.

in both OB and LC. Other mRNAs for pro-inflammatory markers were also dysregulated in OB, HT, raphe, and LC.

Conclusions: Our results suggest that alcohol triggers a compensatory upregulation of ACE2 in the brain due to disturbed RAS and may increase the risk or severity of SARS-CoV-2 infection.

Keywords

SARS-CoV-2; COVID-19; ACE2; Alcohol; Neuroinvasion

1. Introduction

At the onset of the COVID-19 pandemic, respiratory symptoms were the primary concern following infection by severe acute respiratory syndrome coronavirus 2 (SARS-CoV-2). Since the initial observation that anosmia was an early symptom of infection, concern over neurological symptoms such as headache, dizziness, ageusia, ataxia, loss of autonomic respiratory control, lethargy, depression, and anxiety has gained urgency (Haidar et al., 2021; Mao et al., 2020). Direct evidence of SARS-CoV-2 protein in post-mortem brain tissues, as well as increased inflammatory markers and pathology also underscores the potential for CNS invasion and long-term neurological complications. (Bulfamante et al., 2021; Song et al., 2021). With the prevalence of “long covid” and the devastating impact of these neurological symptoms on quality of life, delineating the mechanisms of SARS-CoV-2 pathophysiology in the CNS is now a top priority in COVID-19 research.

Uncovering risk factors and comorbidities that lead to a greater risk of severe infection, development or progression of symptoms, and death has been critical to developing an effective response to the COVID-19 pandemic. Alcohol use disorder (AUD), as well as other substance use disorders (SUD), have been hypothesized to increase the risk of SARS-CoV-2 infection (Althobaiti et al., 2021; Testino, 2020). While limited clinical or epidemiological data are available on the specific contribution of alcohol to disease severity, emerging evidence shows an increased rate of symptomatic SARS-CoV-2 infection (Saurabh et al., 2021) or increased risk of death (Alberca et al., 2021) due to chronic alcohol consumption in infected individuals. Given that chronic alcohol consumption has been linked to increased viral titers, pulmonary pathology, and death from influenza infection (Meyerholz et al., 2008), and is more generally associated with poorer health outcomes, it is necessary to address whether alcohol consumption directly contributes to the severity of SARS-CoV-2 infection.

The primary mediators of SARS-CoV-2 cellular entry, Angiotensin-Converting Enzyme-2 (ACE2), a Renin-angiotensin system (RAS) receptor, and Transmembrane Serine Protease 2 (TMPRSS2), which cleaves its trimeric spike (S) protein prior to viral internalization, have also been linked to alcohol-related pathophysiology. Elevated circulating levels of ACE2 have been detected in AUD subjects (Okuno et al., 1986), while elevated transcript levels of both *ACE2* and *TMPRSS2* have been measured in brain tissues isolated from AUD subjects (Muhammad et al., 2021). Evidence for ACE2 levels broadly impacting the risk of severe infection is supported by findings of increased lung ACE2 expression following nicotine vapor inhalation (Lallai et al., 2021). The mechanism by which ACE2

levels are up-regulated in the alcohol brain has not been delineated, however previous work has shown that the Angiotensin II receptor (RAS harmful axis) is activated during alcohol administration and triggers the pro-inflammatory pathway (Maul et al., 2005). Moreover, Angiotensin II-mediated neuroinflammation is reported widely in the CNS (Gowrisankar and Clark, 2016; Kandalam and Clark, 2010; Quijano et al., 2022; Reeh et al., 2019; Tran et al., 2022). Although there is no definitive evidence that changes in ACE2 levels impact susceptibility to infection, considerable attention has focused on whether ACE2 levels impact severity and health outcomes.

Research on SARS-CoV has shown that ACE2 mediates viral invasion of the CNS via the olfactory bulb (McCray et al., 2007; Netland et al., 2008). In addition, the vagus nerve might provide an additional route of SARS-CoV-2 CNS entry from infected lungs (Bulfamante et al., 2021). Because ACE2 is associated with CNS entry and alcohol consumption has been linked to more severe outcomes, we sought to test whether alcohol consumption would impact ACE2 levels. More specifically, we tested the hypothesis that chronic intermittent ethanol exposure (CIE) would result in increased expression of cell membrane receptor ACE2, TMPRSS2, ADAM17 (ACE2 sheddase), or Cathepsin L (endosomal receptor for SARS-CoV2) in the mouse CNS. After ethanol exposure, we quantified expression levels of these proteins in discrete brain regions associated either with viral entry or that are directly relevant to neurological symptoms of SARS-CoV-2 infection, including locus coeruleus, raphe nuclei, periaqueductal gray, hypothalamus, thalamus, and amygdala. Overall, CIE resulted in the upregulation of ACE2 levels in a subset of these brain regions. Moreover, to understand the underlying mechanism of how alcohol consumption increases the risk of SARS-CoV-2 infection, we measured the mRNA levels of the receptors that are involved in the renin-angiotensin system (RAS) and pro-inflammatory markers that are known to contribute to AUD or SARS-CoV-2 infection. These findings provide a possible mechanism for increased incidence or severity of neurological symptoms associated with SARS-CoV-2 infection in AUD.

2. Materials and methods

2.1. Animals

All experiments were performed on adult male C57BL/6J mice (3-6 months) following the ethical guidelines of NIH guidelines for animal research and approved by the Institutional Animal Care and Use Committee (IACUC) at the University of Iowa. Animals were housed in a ventilated and temperature-controlled vivarium on a standard 12-hour cycle (lights on at 0230) with *ad libitum* access to food (Envigo NIH-31 Modified Open Formula 7913) and water.

2.2. Chronic intermittent ethanol (CIE) exposure

CIE exposure was achieved via vapor inhalation as previously described (Marcinkiewcz et al., 2014). Briefly, mice were placed in standard mouse cages in Plexiglas® vapor chambers (30 × 10 × 15 cm, La Jolla Alcohol Research Inc., La Jolla, CA, USA) and exposed to ethanol volatilized by heating 95% ethanol mixed with fresh air at a rate of ≈10 L/min. To facilitate intoxication and stabilize blood ethanol concentration (BECs), mice were injected

daily with an alcohol dehydrogenase inhibitor, pyrazole (Sigma, St. Louis, MO, USA; dosage: 1 mmol/kg, i.p.), and a loading dose of EtOH (1.57 g/kg) immediately before placement in vapor chambers. Air controls received only pyrazole and were placed in an alternate cage in the same room and exposed to room air. Each cycle of CIE or air exposure lasted 16 h per day (in at 1700 h, out at 0900 h), followed by an 8 h withdrawal for 4 consecutive days of exposure followed by an 80 h withdrawal. This cycle was repeated for a total of 4 weeks and the mice were perfused 80 h after the last cycle to collect brains for further immunostaining procedures. Two additional cohorts were generated to collect fresh brains and were snap-frozen for downstream applications (Western blot and RT-qPCR).

2.3 Reverse Transcriptase-Quantitative PCR (RT-qPCR)

Following the extractions, the brains were dissected to collect the olfactory bulb (OB), hypothalamus (HT), locus coeruleus (LC), and medullary raphe MR; which comprises raphe magnus (RMG), raphe obscurus (ROB). Total RNA from the above-mentioned brain regions was isolated using TRIzol reagent (Ambion, USA) followed by DNA-free™ DNA Removal Kit (Life Technologies, USA) as described previously (Balasubramanian et al., 2021). RNA was quantified using NanoDrop 1000 Spectrophotometer (Thermo Scientific, USA). The reverse transcription was performed using iScript cDNA synthesis kit (Bio-Rad Laboratories, CA, USA) using the thermal profile: 25 °C for 5 min, 45 °C for 20 min, and 95 °C for 1 min. Quantitative reverse transcription PCR (RT-qPCR) for the target gene *β-actin*, *Ace2*, *Adam17,* SARS-CoV-2 entry receptors: *Tmprss2, Cathepsin L;* RAS receptor: *At1r, At2r, Mas1,* and pro-inflammatory markers: *Il-6, Nfkb1, Tnfα., Nlrp3, Stat3* were performed using SYBR green qPCR master mix (Bio-Rad Laboratories, USA) on CFX96™ Real-time-PCR System (Bio-Rad Laboratories, USA). The specific primer sets used for the amplification of target cDNA are listed in Table 1. The thermal profile used for RT-qPCR was as follows: 95 °C for 10 min followed by 40 cycles of 95 °C for 30 s, 60 °C for 30 s, followed by a melt curve analysis profile: 60 °C to 95 °C in 0.5 °C increments at a rate of 5 s/step. Fold changes in the mRNA levels were determined for each gene after normalization to *β-actin* using the $2^{-\Delta\Delta CT}$ method (Schmittgen and Livak, 2008). Results are represented as fold changes in the mRNA levels (± SEM).

2.4 Western Blot

A separate group of mice was decapitated under isoflurane anesthesia to collect brains and serum for western blot experiments as reported previously (Sagarkar et al., 2021; Selvakumar et al., 2020). Briefly, specific brain regions were dissected (OB, HT, LC, and MR) for the western blot of β-actin, ACE2, TMPRSS2, ADAM17, and Cathepsin L. Total protein from all the tissues were isolated using RIPA lysis buffer. The proteins were quantified using the BCA method (ThermoFisher Scientific, USA) and an equal quantity of proteins was resolved in a 10% SDS-PAGE gel. According to the standard procedures, resolved proteins were further transferred to a PVDF membrane (0.45 μm; Millipore, USA) for immunoblotting and the blots were blocked using Starting Block T20 (TBS) Blocking Buffer (ThermoFisher Scientific, USA) for 1 h at room temperature. Further, the membranes were incubated overnight with antibodies specific to ACE2, TMPRSS2, ADAM17, Cathepsin L, and β-actin at 4°C, then incubated with secondary antibodies (IR dye) for 1 h (Table 2). The blots were visualized, and the images were acquired using

Sapphire Biomolecular Imager (Azure Biosystems Inc, USA) at 700 nm and 800 nm. Protein bands were quantified using Image J 1.45 software (National Institutes of Health, Bethesda, MD). The average relative density of the ACE2, TMPRSS2, ADAM17, and Cathepsin L was determined after normalization to β-actin. Results are represented as a mean relative density of the protein levels (± SEM).

2.5 Immunofluorescence

ACE2 expression was quantified across specific brain regions using standard immunofluorescence methods. ACE2 distribution in different cell types in the brain regions was analyzed using immunofluorescence of ACE2 with neuronal (NeuN), microglial (Iba1), and astrocytic (GFAP) markers. Serotonergic or dopaminergic/noradrenergic neuron-specific expression was determined using tryptophan hydroxylase 2 (TPH2) or tyrosine hydroxylase (TH) immunofluorescence, respectively, as markers for identification. Briefly, mice were anesthetized with Avertin and transcardially perfused with phosphate-buffered saline (PBS), followed by 4% paraformaldehyde (PFA). The brains were extracted, post-fixed in PFA overnight, transferred serially to sucrose solutions (10, 20, and 30%), and then cut using a cryomicrotome (Leica Microsystems, Wetzlar, Germany) to a thickness of 20 μm. For each region of interest (ROI), 4-5 sections were used across the rostral-caudal axis. Sections were washed in PBS and permeabilized in 0.5% Triton X-100/PBS for 30 min, followed by blocking in 10% normal donkey serum in 0.1% Triton X-100/PBS and then incubated with the respective primary and secondary antibodies (Table 3) according to standard immunostaining procedures. Images were acquired on an Olympus FV-3000 confocal microscope in 0.5 μm steps and converted to maximum projection images using Image J software. For every ROI, multiple tiles were imaged, and mosaic stitching was performed using FV3000 Multi-Area Time-Lapse (MATL) Software. Images were analyzed by trained researchers blind to experimental conditions for expression parameters in ImageJ (Fiji) software as described previously (Sagarkar et al., 2021). Immuno-colocalization was analyzed by measuring the percentage of co-localization area pixels by total immunoreactive area pixels after setting color thresholding parameters in ImageJ (Fiji). All the results analyzed were represented as mean percentage immunoreactive area (±SEM). To measure the degree of colocalization between ACE2 and neuronal markers, the Pearson correlation coefficient (PCC) and Mander's overlap coefficient (MOC) was calculated using the Just Another Colocalization plugin (JACoP) in ImageJ (Fiji) for all the colocalization analyses (Dunn et al., 2011). The results for both coefficients were represented as the mean of the correlation coefficient values (±SEM).

2.6 Data and statistical analysis

The statistical analysis was performed using GraphPad Prism 9 (CA, USA). The significance of differences between the two groups (Air control vs. CIE) was assessed using the Student's Unpaired t-test with Welch's correction. A p-value less than 0.05 was considered significant for all the analyses. In addition, % change among the group was also calculated for all the measures. All the statistical information is mentioned in the supplementary tables (Table S1-S9).

3. Results

3.1 Alcohol exposure impacts ACE2 expression in the mouse olfactory bulb

Our initial results show widespread ACE2 expression across brain regions, but more limited TMPRSS2 expression (Supplementary Figure 1), and the ACE2 levels were increased in the serum using ELISA and Western blot (Supplementary Figure 2A,B). Next, we turned to immunofluorescent labeling of mouse brain sections to quantify ACE2 and TMPRSS2 expression patterns with finer spatial resolution. Consistent with data from Supplementary Figure 1, we observe robust ACE2 expression throughout the mouse OB (Figure 1A) using immunofluorescence staining. Like in serum, ACE2 expression significantly increased in the OB following CIE ($p = 0.0220$; Figure 1A-C). Western blot of ACE2 showed two fractions: a transmembrane protein (cACE2) and a soluble catalytic ectodomain (sACE2). sACE2 levels in the OB were increased significantly ($p = 0.0136$) following CIE, however, cACE2 wasn't altered (Figure 1G). We also analyzed the effect of CIE on ADAM17, a sheddase protease that proteolytically cleaves ACE2 to sACE2 (Zipeto et al., 2020). sACE2 protein levels were increased in the OB coherently with ADAM17 following CIE ($p = 0.0136$, sACE2, Figure 1G; $p = 0.0136$, ADAM17, Figure 1H). Our data also show expression of TMPRSS2 throughout the OB (Figure 1D), but no change in expression was observed using immunofluorescence (Figure 1E and 1F) and Western blot (Figure 1H) following CIE. However, endosomal Cathepsin L protein levels were increased ($p = 0.0241$) in the OB following alcohol exposure suggesting that the CIE might increase the risk for endosomal entry of SARS-CoV-2 (Figure 1H). Moreover, we also analyzed the mRNA levels of ACE2, TMPRSS2, ADAM17, and Cathepsin L, but no change was observed following CIE (Figure 1I).

3.2 Alcohol exposure increased ACE2 levels in discrete hypothalamic regions

The spread of viral expression into several hypothalamic regions has also been reported following viral entry into the OB (Netland et al., 2008). Hypothalamic projections from the olfactory bulb could mediate this route of viral invasion (Papp, 2014). With these findings in mind, we tested for differential ACE2 expression levels in discrete hypothalamic regions following CIE. Figure 2 shows robust ACE2 immunolabeling in the paraventricular nucleus of the hypothalamus (PVN) (Figure 2A,D), the lateral hypothalamus (LH) (Figure 2B,E), or the arcuate nucleus (ARC) (Figure 2C,F). Consistent with our observations in the OB, we observed a significant increase in ACE2 expression in both the PVN ($p = 0.0424$) and LH ($p = 0.0100$) but observed no changes in the ARC ($p = 0.1449$; Figure 2G-I). We also observed heightened levels of sACE2 ($p = 0.0234$) and a trend toward an increase in cACE2 levels by Western blot following CIE ($p = 0.0876$; Figure 2J). Moreover, we also observed heightened mRNA levels of ACE2 following CIE ($p = 0.037$, Figure 2L) similar to Western blot and immunofluorescence. ADAM17 protein levels were also increased significantly ($p = 0.0418$, Figure 2K), which can be related to higher sACE2 in CIE mice. While TMPRSS2 was increased following CIE ($p = 0.037$, Figure 2K), no change was observed in the Cathepsin L expression in the hypothalamus.

3.3 Differential expression of ACE2 in serotonergic raphe nuclei following CIE exposure

We expanded our investigation into regions that could underlie the neurological symptoms associated with SARS-CoV-2. Serotonergic nuclei have reciprocal projections with the hypothalamus (Papp, 2014), and dysfunction in these nuclei is associated with neurological and affective changes. Therefore, we tested whether dorsal raphe nucleus (DRN) serotonergic neurons are vulnerable to changes in *ACE2* or *TMPRSS2* expression following CIE vapor treatment. We labeled serotonergic neurons by immunostaining for 5-hydroxytryptamine (5-HT) and co-labeled for ACE2 or TMPRSS2 (Figure 3A-T). While we observe ACE2 and TMPRSS2 expression throughout the DRN, only a subset of serotonergic neurons shows co-labeling for either protein. Further, we observe substantial ACE2 and TMPRSS2 expression in other cell types. In the DRN, we also observe a significant increase in 5-HT immunostaining ($p = 0.0251$) and a trend toward increased ACE2 % immunoreactive area ($p = 0.0614$), but no significant changes in TMPRSS2 ($p = 0.7964$; Figure 3U) after CIE. Further analysis reveals a significant increase in 5HT/ACE2 colocalization by % immunoreactive area ($p = 0.0354$; Figure 3V) and increased Pearson correlation coefficient ($p = 0.0118$; Figure 3W). Quantification of Mander's overlap coefficient also shows a significant increase in ACE2/5HT colocalization, indicating increased ACE2 expression in 5-HT neurons (M2, $p = 0.0117$; Figure 3X).

While the DRN comprises a majority of CNS 5-HT neurons, ACE2 expression in the medullary serotonergic nuclei is highly relevant to SARS-CoV-2 infection as the brainstem is vulnerable to SARS-CoV-2 neuroinvasion (Bulfamante et al., 2021). We next tested whether CIE exposure impacts ACE2 expression levels in the raphe magnus. Here we labeled serotonergic neurons using an anti-TPH2 antibody (Figure 4A). We also observed robust ACE2 expression in the RMG, some of which localizes to cells with neuronal morphology (Figure 4B). As in the DRN, ACE2 is expressed in a subset of RMG serotonergic neurons, with other cell types comprising the remainder of the immunolabeling (Figure 4C). Unlike the DRN, ethanol vapor exposure increased ACE2 % immunoreactive area ($p = 0.0153$; Figure 4E, 4G) and decreased TPH2 immunoreactive area ($p = 0.05$; Figure 4D, 4G). Quantification of immunofluorescence also revealed a significant decrease in TPH2/ACE2 co-localization following CIE ($p = 0.0031$; Figure 4F, 4H). Further analysis revealed no change in the Pearson correlation coefficient ($p = 0.1438$; Figure 4I), but a significant decrease in the Mander's overlap coefficient for ACE2 and TPH2 co-expression (M2, $p = 0.0349$; Figure 4J).

Figure 5 shows similar results for the ROB, another medullary serotonergic nucleus. ROB functions include regulation of breathing and gut motility, both of which are highly relevant to SARS-CoV-2 symptoms. Neuronal projections to the lungs or gut have also been proposed as a route for CNS viral entry (Lima et al., 2020). In Figure 5, we quantified ACE2 expression and tested whether CIE impacted localization in the ROB. We observe robust TPH2 immunolabeling of serotonergic neurons (Figure 5A) and ACE2 expression (Figure 5B). Only a subset of serotonergic neurons in the ROB express ACE2, but ACE2 labeling was also widely observed in non-serotonergic cells (Figure 5C). Based on cellular morphology, other neuronal populations in the ROB potentially express ACE2. Following CIE, TPH2 and ACE2-mediated immunofluorescence increased significantly (Figure 5D and

E, respectively), as quantified in Figure 5G ($p = 0.0234$ for ACE2 and $p = 0.0051$ for TPH2). In addition to an increase in overall levels, we also see increases in metrics of co-expression, including % immunoreactive area ($p = 0.0230$; Figure 5F, 5H), increased Pearson correlation coefficient ($p = 0.0127$; Figure 5I), and both Mander's overlap coefficients (Figure 5J; $p = 0.0193$ and $p = 0.0243$ for M1 and M2, respectively).

We pooled the tissue from raphe magnus and obscurus to quantitate the protein and mRNA levels for ACE2 using western blot and RT-qPCR respectively. The western blot showed a trend toward an increase in cACE2 levels (Figure 5K), while no change was observed in the sACE2 levels. On the contrary, the RT-qPCR showed a decrease in the ACE2 mRNA expression following alcohol exposure ($p = 0.022$; Figure 5L). Moreover, the mRNA levels of other receptors ADAM17 and TMPRSS2 didn't alter, however, Cathepsin L was decreased on alcohol exposure ($p = 0.0002$; Figure 5L). Altogether the protein and mRNA levels in the medullary raphe suggest that the increase in ACE2 is more relevant to the cellular form and not the soluble form and this could be due to undetected ADAM17 and unaltered TMPRSS2.

3.4 Impact of alcohol exposure on expression levels in noradrenergic locus coeruleus

Next, we turned our attention to the LC, the primary source of noradrenergic neurons in the CNS which receives projections from the DRN. We identified noradrenergic neurons by labeling for tyrosine hydroxylase (TH; Figure 6A). Again, we observed ACE2 immunolabeling throughout the LC and in a subset of TH-positive cells (Figure 6B and C, respectively). Following chronic ethanol exposure, we saw increased labeling of both TH and ACE2 in the locus coeruleus (Figure 6D and E, respectively). Although ACE2 continued to be expressed in TH-positive neurons, there was no indication that this increase in expression was limited to noradrenergic neurons (Figure 6F). Quantification of immunolabeling (Figure 6G) indicates an increased ACE2 expression ($p = 0.0102$) and TH expression ($p = 0.0266$). Analysis of co-localized area (6H) or Pearson correlation coefficient (6I) did not indicate any changes in co-expression ($p = 0.1377$ and $p = 0.1737$, respectively). However, Mander's overlap analysis indicates that a significant increase in ACE2 expression occurs within TH-positive cells, with a trend toward increased M1 coefficient ($p = 0.0609$) and a significant increase in M2 coefficient ($p = 0.0434$; Figure 6J). Moreover, we analyzed the levels of cACE2 and sACE2 by Western blot in LC and found that cACE2 wasn't altered whereas sACE2 was increased significantly in the CIE group ($p = 0.032$, Figure 6K). Consistent with our observation in the immunofluorescence and Western blot analyses, we also observed that ACE2 mRNA expression was higher in the CIE mice as compared to the air controls ($p = 0.018$, Figure 6M). We also quantified TMPRSS2 and Cathepsin L protein levels by Western blot and observed that TMPRSS2 was increased significantly in the CIE group ($p = 0.0078$, Figure 6L), but no change was observed in the Cathepsin L protein levels. Overall, these data show that ACE2 expression in the LC significantly increases following CIE exposure, and the viral internalization might be through TMPRSS2 and not by endosomal Cathepsin L.

3.5 ACE2 levels in the PAG are increased following CIE exposure

The periaqueductal grey (PAG) is vulnerable to SARS-CoV infection and impacts critical autonomic functions such as heart rate and breathing (Faull et al., 2019). In investigating this brain region, our initial results showed ACE2 is also expressed in the ventral/lateral (Figure 7A) and dorsal/medial PAG (Figure 7B). We then tested whether ACE2 levels were also increased in this midbrain locus following CIE. Our results indicate a significant increase in % ACE2 immunoreactive area in the ventral/lateral PAG (Figure 7C,D) and a trend toward increased expression in the dorsal/medial PAG (Figure 7E,F; $p = 0.0393$ and $p = 0.0577$, respectively).

3.6 Reduced ACE2 levels in Amygdala following chronic ethanol exposure

Finally, we considered whether alcohol exposure impacts ACE2 expression in the paraventricular thalamus (PVT) and amygdala (AMY). Both brain regions receive extensive sensory input and projections from other brain regions. The thalamus is a key node in multiple neuronal circuits and is highly vulnerable to damage from chronic ethanol consumption (Segobin et al., 2019). In both brain regions, we observed robust baseline levels of ACE2 (Figure 8A and D) in control mice. Surprisingly, we saw a trend toward decreased ACE2 expression in the PVT following alcohol exposure ($p = 0.0704$; Figure 8B,C) and significantly lower ACE2 levels in the AMY ($p = 0.0364$; Figure 8E,F).

3.7 ACE2 expression in different cell types of the raphe nuclei

Our results so far have implicated that the ACE2 is expressed in monoaminergic neurons and is altered after CIE exposure. We also noticed ACE2 expression in other cells of medullary raphe (MR; RMG and ROB) and hypothalamic regions (PVN, ARC, and LH) that are not monoaminergic. We then co-stained ACE2 with a neuronal (NeuN), astrocytic (GFAP), and microglial (Iba1) marker in the hypothalamic (PVN, ARC, LH) and raphe (RMG and ROB) nuclei. The immunofluorescent staining showed that ACE2 is expressed abundantly in neurons and is also expressed to an extent in microglia. However, no signs of ACE2 in astrocytes were observed in these regions (MR: Figure 9A-J). Similar observations were also noticed in the hypothalamic nuclei (PVN, ARC, LH; Supplementary Figure 3).

3.8 Impact of alcohol exposure on mRNA expression levels of the receptors of the RAS pathway

The binding of angiotensin II to the receptor (AT1R or AT2R) induces a pro-inflammatory signaling cascade, while the binding of angiotensin (1-7) to the MAS1 receptor initiates an anti-inflammatory signaling pathway. The homeostasis between these pathways is regulated by ACE2 which cleaves angiotensin II to angiotensin (1-7) (Burrell et al., 2004). To understand the underlying mechanism for the CIE-induced increase in ACE2 expression, we measured mRNA expression levels of the receptors of the RAS pathway (*At1r, At2r, and Mas1*) in the OB, HT, MR, and LC. The mRNA levels of *At1r* and *At2r* were reduced in the OB ($p = 0.002$ for *At1r* and $p = 0.024$ for *At2r*; Figure 10A) and increased in LC ($p = 0.014$ for AT1R and $p = 0.002$ for AT2R; Figure 10G). However, in the HT, the RT-qPCR showed an increasing trend for the *At1r* mRNA (Figure 10C) and no change in the MR. Likewise, the *Mas1* receptor was increased significantly in the OB ($p = 0.020$; Figure 10A) and LC (p

= 0.020; Figure 10G) following CIE, and no change was observed in the MR (Figure 10C). However, mRNA levels show an increasing trend of *Mas1* expression in the HT following CIE ($p = 0.097$; Figure 10B). Overall, the RT-qPCR data suggest that the CIE induces an increase in the pro-inflammatory RAS pathway, which in turn upregulates ACE2 levels in the brain to initiate compensatory anti-inflammatory RAS signaling.

3.9 Impact of alcohol exposure on the mRNA expression of the pro-inflammatory markers

To further understand CIE-induced dysregulation of the RAS pathway and the downstream activation of pro-inflammatory signaling, we analyzed mRNA levels of key pro-inflammatory markers (*Il-6, Nfkb, Tnfα, Nlrp3, and Stat3*) that are involved in SARS-CoV-2 etiology (Jiang et al., 2022). *Il-6* was increased significantly in the OB ($p = 0.044$; Figure 10B) and locus coeruleus ($p = 0.003$; Figure 10H) following CIE and no change was observed in the HT and MR (Figure 10D, F). *Nfkb1* was decreased in the OB ($p = 0.043$) and remained unaltered in other regions tested (Figure 10B, D, F, H). *Tnfα* was decreased in the HT ($p = 0.031$; Figure 10D) and MR ($p = 0.002$; Figure 10F), increased in LC ($p = 0.042$; Figure 10H), and unaltered in the OB following CIE. *Nlrp3* mRNA expression was increased significantly in the HT ($p = 0.046$; Figure 10D) and MR ($p = 0.032$; Figure 10F), and no change was observed in the OB and LC (Figure 10B, H) following CIE. The transcription factor *Stat3* was increased significantly in LC ($p = 0.023$; Figure 10H) and decreased in the OB ($p = 0.030$; Figure 10B), HT ($p = 0.019$; Figure 10D), and MR ($p = 0.045$; Figure 10F).

4. Discussion

While SARS-CoV-2 respiratory infection and related complications have driven hospitalizations and mortality and were the primary focus early in the pandemic, a significant proportion of infections result in extensive neurological symptoms. Furthermore, accumulating evidence shows that SARS-CoV-2 invasion of the CNS underlies neurological complications (Siddiqui, 2021). Previous work shows the SARS-CoV-2-associated genes *ACE2* and *TMPRSS2* were upregulated in the frontal and motor cortex of chronic AUD patients (Muhammad et al., 2021). In the present study, we examined a larger set of brain regions for the expression of *ACE2* in mice exposed to 4 weeks of CIE. Our results show that ACE2 levels were altered after CIE in the OB, HT, AMY, and monoaminergic brainstem regions. The relevance of monoamine neuron function to addiction is well established (Jaatinen et al., 2013; Marcinkiewcz et al., 2016a), but altered ACE2 levels in these neurons may also heighten the severity of SARS-CoV-2 infection after chronic alcohol exposure. Elevated ACE2 in the OB, HT, and brainstem might increase the risk of neuroinvasion, while infection of monoaminergic neurons could augment the spread via the widespread network of serotonergic and noradrenergic projections throughout the brain. Altered activity or loss of these neurons may also account for increasing reports of neuropsychiatric complications in the wake of COVID-19 infection.

4.1 Alcohol alters the ACE2 expression in the SARS-CoV-2 entry points- the olfactory bulb and hypothalamus

RT-qPCR and Western blot data showing widespread ACE2 expression in the current study are consistent with previous findings (Doobay et al., 2007; Qiao et al., 2020). ACE2 exists as a transmembrane protein (cACE2) and as a soluble catalytic ectodomain (sACE2), detectable in CSF (García-Escobar et al., 2021). Interestingly, we detected differential expression of sACE2 in several brain regions with elevated ACE2 immunoreactivity that were accompanied by elevated TMPRSS2 and/or ADAM17, which cleave cACE2 to generate sACE2 (Heurich et al., 2014). The suggested mechanisms for coronavirus propagation within the brain include internalization in nerve terminals by endocytosis, retrograde transportation, axonal transport, and transsynaptic mode of spreading (Dubé et al., 2018), so high levels of sACE2 in brain regions such as the olfactory bulb and hypothalamus may help SARS-CoV-2 propagate into other brain regions.

COVID-19 patients display anosmia as an early indication of infection. Growing evidence of ACE2 expression in the OB confirms the intranasal/olfactory system route is highly relevant to SARS-CoV-2 CNS invasion (Jiao et al., 2021; Qiao et al., 2020; Song et al., 2021; Ueha et al., 2020). An intranasal administration of SARS-CoV-2 in h*ACE2* mice further confirms an infection in sustentacular cells and olfactory neurons (Tang et al., 2021). Interestingly, we observed an increase in sACE2 levels and a non-significant change in TMPRSS2 after CIE. However, the endosomal receptor Cathepsin L was increased following CIE, suggesting that CIE might increase the risk for endosomal entry of SARS-CoV-2.

Identification of the SARS-CoV genome in the hypothalamus has also been reported following viral entry into the OB (Netland et al., 2008). Since acute and chronic exposure to alcohol has direct or indirect effects on endocrine functions, which are mediated by the HPA axis (Rachdaoui and Sarkar, 2017), we examined ACE2 levels in various hypothalamic nuclei and observed an increase in the LH and PVN following CIE. Moreover, sACE2 levels were increased along with ADAM17 and TMPRSS2 in the hypothalamus. The hypothalamus integrates information from almost all regions of the brain, in particular the brainstem, upon receiving peripheral sensory inputs from different sources including the olfactory system (Papp, 2014).

4.2 Alcohol alters ACE2 expression in monoaminergic brainstem nuclei

Most serotonergic neurons arise from the DRN, which spans the midbrain and brainstem and plays a significant role in the etiology of neuropsychiatric disorders and AUD (Marcinkiewcz, 2015). Following CIE, we observed an increase in 5-HT levels in the DRN in accordance with a previous study reporting hyperexcitability of DRN neurons after CIE vapor (Lowery-Gionta et al., 2014). Our results also align with a post-mortem study indicating greater TPH immunoreactivity in alcohol-dependent individuals throughout the rostral-caudal axis of DRN (Underwood et al., 2007). The DRN is also known to participate in modulating the core respiratory networks of the brainstem (Smith et al., 2018), and a recent report indicates the expression of ACE2 in 5-HT neurons in the DRN of rats (Hernández et al., 2021). We examined ACE2 and TMPRSS2 levels in DRN and found that while global ACE2 expression did not change significantly, there was a significant increase

in ACE2 colocalization with 5-HT neurons. Although there was no significant change in TMPRSS2 after CIE exposure, the caudal region showed a significant colocalization of 5-HT and TMPRSS2.

A clinical study reported immunoreactivity for nucleoprotein (NP) of SARS-CoV-2 in neurons and glial cells of respiratory centers of the brainstem and medulla (Bulfamante et al., 2021). In addition, vagus nerve afferent fibers in the medulla of COVID-19 patients showed intense NP immunostaining, arguing for viral trafficking between the brainstem and the lung or gut. The present study confirms the prominent expression of ACE2 in serotonin and non-serotonin neurons in the raphe magnus and obscurus/palladium. It is worth noting that ACE2 expression in these regions was highly conspicuous as compared to the DRN and was significantly increased after CIE exposure. Altogether, it is conclusive that ACE2 is prominently expressed in the medullary raphe nucleus and is a viable candidate for SARS-CoV-2 neuroinvasion via the vagal nerve. Interestingly, TPH2 expression was bidirectionally modulated by CIE in these nuclei, with an increase in the TPH2-immunoreactivity in obscurus/palladium and a decrease in the magnus. Because of the difference in the TPH2-immunoreactive area in these regions, the number of TPH2 neurons expressing ACE2 was greater in obscurus/palladium and lesser in magnus in CIE mice. To our knowledge, this is the first report of the effects of chronic alcohol on these medullary raphe nuclei in adult animals.

Noradrenergic neurons in the LC have been associated with a wide array of physiological functions including cardiovascular and respiratory control (de Carvalho et al., 2017) via direct projections to the spinal cord or projections to autonomic nuclei (Samuels and Szabadi, 2008). As autonomic functions are impaired in COVID-19 patients after infection (Becker, 2021) and the LC is one of the regions that is associated with these functions, we tested ACE2 immunoreactivity in LC neurons after CIE exposure. Many TH-positive neurons in the LC were positive for ACE2 expression as previously reported (Hernández et al., 2021) and the number of TH-ACE2 neurons was increased in CIE mice, suggesting an increased vulnerability of LC neurons to SARS-CoV-2 infection. More specifically, sACE2 levels were increased in the LC with an increase in the sheddase or viral internalizing protein TMPRSS2. The increase in TH expression in LC could be the effect of “kindling” caused by repeated withdrawals of substances as previously reported (Fitzgerald, 2013).

The PAG is another brainstem region that also plays a critical role in autonomic function, especially breathing (Faull et al., 2019), and shows increased viral antigen for SARS-CoV in h*ACE2* mice after 3 days of intranasal inoculation (Netland et al., 2008). Moreover, acute and chronic alcohol exposure is known to induce robust enhancement of glutamatergic synaptic transmission in dopamine neurons of the VL-PAG (Li et al., 2013). We then investigated the effects of CIE on the ACE2 expression levels in VL-PAG and DM-PAG and found that ACE2 levels were increased significantly in the VL-PAG, suggesting that alcohol can potentiate the vulnerability of this region to viral infection.

4.3 Alcohol impacts ACE2 expression in brain regions associated with sensory stimuli and emotional valence

The thalamus is a structure of the diencephalon that has extensive nerve connections to the brainstem and the cerebral cortex and is functionally involved in transmitting sensory information to the cortex. A few clinical reports have shown a significant role of the thalamus in encephalitis after viral infection (Abel et al., 2020). Moreover, thalamic abnormalities are a key feature in alcohol-related brain dysfunction. In the present study, we observe decreased ACE2 levels in the PVT following CIE. However, it is possible that this reduction in ACE2 could be due to shrinkage of the thalamus as previously reported in clinical studies of alcohol dependence (Pitel et al., 2015).

Besides the brainstem and hypothalamus, ACE2 was also highly expressed in the amygdala (Piras et al., 2021), a brain region implicated in anxiety, stress-related disorders, and the reinforcing effects of alcohol and other drugs of abuse (Roberto et al., 2021). Moreover, RNA-sequencing analysis of the amygdala tissue of COVID-19 patients displays upregulation of interferon-related neuroinflammation genes as well as downregulation of synaptic and other neuronal genes (Piras et al., 2021). Based on COVID-19 reports and the significance of amygdalar circuits in alcohol dependence, we measured ACE2 levels in the amygdala of CIE mice and found that they decreased after exposure. Amygdalar ACE2 is known to reduce anxiety by activating MAS receptor signaling (Wang et al., 2016), which is a potential mechanism for observations of increased anxiety in mice after CIE.

4.4 Mechanistic interpretation of alcohol exposure and increased risk of SARS-CoV-2 infection

To reconcile the overall mechanism of how ethanol intoxication increases ACE2 levels in the brain, we suggest that heightened levels of sACE2 and ADAM17 (sheddase) in the CNS could be due to an environment with high levels of Angiotensin II, which initiates a pro-inflammatory cascade via AT1R. These pro-inflammatory mediators, in turn, may upregulate gene expression of ACE2 and ADAM17 (Clarke et al., 2014). This is perhaps because sACE2 which retains its catalytic activity can easily access and cleave Angiotensin II to Angiotensin 1-7 (Zipeto et al., 2020). Therefore, an increase in sACE2 indicates that Angiotensin II is elicited under CIE conditions, and sACE2 is shed by ADAM17 to counterbalance the harmful effects of the RAS pathway. In line with this, previous reports show that transgenic rats expressing antisense RNA against Angiotensin II consumed less alcohol as compared to wild-type controls and indicated that the central effect of Angiotensin II on alcohol consumption is mediated by angiotensin receptor AT1R (Maul et al., 2005). An increase in MAS1 receptor after CIE in the current study is another indication for the deregulation of the RAS pathway, where MAS1 levels are heightened to meet the requirement of the cell to counterbalance higher Angiotensin II levels and initiate anti-inflammatory pathways as a response to a harmful pro-inflammatory signal triggered by AT1R and AT2R.

Several studies have reported sACE2 as a decoy receptor and showed its beneficial and protective role in therapeutics for COVID-19 (Pang et al., 2020; Tang et al., 2020). Surprisingly, clinical information suggests that patients with low cACE2 and high sACE2

had a poorer prognosis (Basit et al., 2021), conflicting with the therapeutic potential of sACE2. Based on our data and recent reports (Rahman et al., 2021), we suggest that the increase in sACE2 is a response to heightened Angiotensin II in AUD patients and this might elevate the risk of SARS-CoV-2 infection, leading to depletion of cACE2 and sACE2 by forming an ACE2-virus complex (Figure 11). This in turn exacerbates RAS homeostasis thereby increasing Angiotensin II levels and leading to a cytokine storm (Mahmudpour et al., 2020; Tran et al., 2022) and other pathological complications (Kai and Kai, 2020).

It is known that Angiotensin II activates JAK2/STAT3 pathway and induces IL-6 and NFkB production in cultured rat brainstem cells (Gowrisankar and Clark, 2016; Kandalam and Clark, 2010), and this aligns with our observation of increased STAT3, IL-6 and NFkB mRNA levels in the LC after CIE. However, IL-6 was increased in the OB with a drop in STAT3 levels, which could be due to the feedback inhibition of the IL-6 classical pathway (Reeh et al., 2019). Moreover, in the HT and MR nuclei, NLRP3 was increased after CIE due to the activation of the Angiotensin II-AT1R-mediated pro-inflammatory pathway as noticed before in the substantia nigra of aging and PD models (Quijano et al., 2022).

Altogether, our study provides evidence that chronic alcohol exposure and withdrawal increases ACE2 levels in monoaminergic neuronal circuits and may potentiate the risk of CNS-viral entry as well as cardiovascular, respiratory, and neuropsychiatric complications. We also conclude that the increase in sACE2 levels is a sign of chronic RAS-AT1R activation that potentiates pro-inflammatory signaling in AUDs, and that ACE2 may act as a molecular brake on excessive neuroinflammation. While this study provides a mechanism for increased SARS-CoV-2 severity in individuals who chronically consume alcohol, it represents only an indirect sign of potential vulnerability. Follow-up research is needed to directly show that ethanol-dependent changes in ACE2 levels impact SARS-CoV-2 CNS invasion, disease severity, or prevalence of neurological symptoms.

Supplementary Material

Refer to Web version on PubMed Central for supplementary material.

Acknowledgments

This work was funded through NIH grants R00 AA024215, R00 AA024215-04S2, and R00 AA024215-04S1 to C.M. T.J. was supported by T32 HL007638-35. We thank Yu Xu for performing the animal experiments.

References

Abel D, Shen MY, Abid Z, Hennigan C, Boneparth A, Miller EH, Uhlemann A-C, McBrian DK, Thakur K, Silver W, Bain JM (2020) Encephalopathy and bilateral thalamic lesions in a child with MIS-C associated with COVID-19. Neurology 95:745–748. [PubMed: 32847953]

Alberca RW, Rigato PO, Ramos YÁL, Teixeira FME, Branco ACC, Fernandes IG, Pietrobon AJ, Duarte AJ da S, Aoki V, Orfali RL, Sato MN (2021) Clinical Characteristics and Survival Analysis in Frequent Alcohol Consumers With COVID-19. Front Nutr.

Althobaiti YS, Alzahrani MA, Alsharif NA, Alrobaie NS, Alsaab HO, Uddin MN (2021) The possible relationship between the abuse of tobacco, opioid, or alcohol with covid-19. Healthcare (Switzerland).

Balasubramanian N, Sagarkar S, Choudhary AG, Kokare DM, Sakharkar AJ (2021) Epigenetic Blockade of Hippocampal SOD2 Via DNMT3b-Mediated DNA Methylation: Implications in Mild Traumatic Brain Injury-Induced Persistent Oxidative Damage. Mol Neurobiol 58:1162–1184. [PubMed: 33099744]

Basit A, Ali T, Rehman SU (2021) Truncated human angiotensin converting enzyme 2; a potential inhibitor of SARS-CoV-2 spike glycoprotein and potent COVID-19 therapeutic agent. J Biomol Struct Dyn 39:3605–3614. [PubMed: 32396773]

Becker RC (2021) Autonomic dysfunction in SARS-COV-2 infection acute and long-term implications COVID-19 editor's page series. J Thromb Thrombolysis 52:692–707. [PubMed: 34403043]

Bulfamante G, Bocci T, Falleni M, Campiglio L, Coppola S, Tosi D, Chiumello D, Priori A (2021) Brainstem neuropathology in two cases of COVID-19: SARS-CoV-2 trafficking between brain and lung. J Neurol.

Burrell LM, Johnston CI, Tikellis C, Cooper ME (2004) ACE2, a new regulator of the renin–angiotensin system. Trends in Endocrinology & Metabolism 15:166–169. [PubMed: 15109615]

Clarke NE, Belyaev ND, Lambert DW, Turner AJ (2014) Epigenetic regulation of angiotensin-converting enzyme 2 (ACE2) by SIRT1 under conditions of cell energy stress. Clin Sci 126:507–516.

de Carvalho D, Patrone LGA, Marques DA, Vicente MC, Szawka RE, Anselmo-Franci JA, Bícego KC, Gargaglioni LH (2017) Participation of locus coeruleus in breathing control in female rats. Respir Physiol Neurobiol 245:29–36. [PubMed: 28687484]

Doobay MF, Talman LS, Obr TD, Tian X, Davisson RL, Lazartigues E (2007) Differential expression of neuronal ACE2 in transgenic mice with overexpression of the brain renin-angiotensin system. American Journal of Physiology-Regulatory, Integrative and Comparative Physiology 292:R373–R381. [PubMed: 16946085]

Dubé M, Le Coupanec A, Wong AHM, Rini JM, Desforges M, Talbot PJ (2018) Axonal Transport Enables Neuron-to-Neuron Propagation of Human Coronavirus OC43. J Virol 92.

Dunn KW, Kamocka MM, McDonald JH (2011) A practical guide to evaluating colocalization in biological microscopy. American Journal of Physiology-Cell Physiology 300:C723–C742. [PubMed: 21209361]

Faull OK, Subramanian HH, Ezra M, Pattinson KTS (2019) The midbrain periaqueductal gray as an integrative and interoceptive neural structure for breathing. Neurosci Biobehav Rev 98:135–144. [PubMed: 30611797]

Fitzgerald PJ (2013) Elevated Norepinephrine may be a Unifying Etiological Factor in the Abuse of a Broad Range of Substances: Alcohol, Nicotine, Marijuana, Heroin, Cocaine, and Caffeine. Subst Abuse 7:SART.S13019.

García-Escobar A, Jiménez-Valero S, Galeote G, Jurado-Román A, García-Rodríguez J, Moreno R (2021) The soluble catalytic ectodomain of ACE2 a biomarker of cardiac remodelling: new insights for heart failure and COVID19. Heart Fail Rev 26:961–971. [PubMed: 33404999]

Gowrisankar Y v., Clark MA (2016) Angiotensin II induces interleukin-6 expression in astrocytes: Role of reactive oxygen species and NF-κB. Mol Cell Endocrinol 437:130–141. [PubMed: 27539920]

Haidar MA, Jourdi H, Haj Hassan Z, Ashekyan O, Fardoun M, Wehbe Z, Maaliki D, Wehbe M, Mondello S, Abdelhady S, Shahjouei S, Bizri M, Mechref Y, Gold MS, Dbaibo G, Zaraket H, Eid AH, Kobeissy F (2021) Neurological and Neuropsychological Changes Associated with SARS-CoV-2 Infection: New Observations, New Mechanisms. The Neuroscientist 107385842098410.

Hernández VS, Zetter MA, Guerra EC, Hernández-Araiza I, Karuzin N, Hernández-Pérez OR, Eiden LE, Zhang L (2021) ACE2 expression in rat brain: Implications for COVID-19 associated neurological manifestations. Exp Neurol 345:113837. [PubMed: 34400158]

Heurich A, Hofmann-Winkler H, Gierer S, Liepold T, Jahn O, Pöhlmann S (2014) TMPRSS2 and ADAM17 Cleave ACE2 Differentially and Only Proteolysis by TMPRSS2 Augments Entry Driven by the Severe Acute Respiratory Syndrome Coronavirus Spike Protein. J Virol 88:1293–1307. [PubMed: 24227843]

Jaatinen P, Sarviharju M, Raivio N, Eriksson C, Hervonen A, Kiianmaa K (2013) Effects of Lifelong Ethanol Consumption on Brain Monoamine Transmitters in Alcohol-Preferring Alko Alcohol (AA) Rats. Brain Sci 3:790–799. [PubMed: 24961425]

Jiang Y, Rubin L, Peng T, Liu L, Xing X, Lazarovici P, Zheng W (2022) Cytokine storm in COVID-19: from viral infection to immune responses, diagnosis and therapy. Int J Biol Sci 18:459–472. [PubMed: 35002503]

Jiao L, Yang Y, Yu W, Zhao Y, Long H, Gao J, Ding K, Ma C, Li J, Zhao S, Wang H, Li H, Yang M, Xu J, Wang J, Yang J, Kuang D, Luo F, Qian X, Xu L, Yin B, Liu W, Liu H, Lu S, Peng X (2021) The olfactory route is a potential way for SARS-CoV-2 to invade the central nervous system of rhesus monkeys. Signal Transduct Target Ther 6:169. [PubMed: 33895780]

Kai H, Kai M (2020) Interactions of coronaviruses with ACE2, angiotensin II, and RAS inhibitors—lessons from available evidence and insights into COVID-19. Hypertension Research 43:648–654. [PubMed: 32341442]

Kandalam U, Clark MA (2010) Angiotensin II activates JAK2/STAT3 pathway and induces interleukin-6 production in cultured rat brainstem astrocytes. Regul Pept 159:110–116. [PubMed: 19748527]

Lallai V, Manca L, Fowler CD (2021) E-cigarette vape and lung ACE2 expression: Implications for coronavirus vulnerability. Environ Toxicol Pharmacol.

Li C, McCall NM, Lopez AJ, Kash TL (2013) Alcohol effects on synaptic transmission in periaqueductal gray dopamine neurons. Alcohol 47:279–287. [PubMed: 23597415]

Lima M, Siokas V, Aloizou AM, Liampas I, Mentis AFA, Tsouris Z, Papadimitriou A, Mitsias PD, Tsatsakis A, Bogdanos DP, Baloyannis SJ, Dardiotis E (2020) Unraveling the Possible Routes of SARS-COV-2 Invasion into the Central Nervous System. Curr Treat Options Neurol.

Lowery-Gionta EG, Marcinkiewcz CA, Kash TL (2015) Functional Alterations in the Dorsal Raphe Nucleus Following Acute and Chronic Ethanol Exposure. Neuropsychopharmacology 40:590–600. [PubMed: 25120075]

Mahmudpour M, Roozbeh J, Keshavarz M, Farrokhi S, Nabipour I (2020) COVID-19 cytokine storm: The anger of inflammation. Cytokine 133:155151. [PubMed: 32544563]

Mao L, Jin H, Wang M, Hu Y, Chen S, He Q, Chang J, Hong C, Zhou Y, Wang D, Miao X, Li Y, Hu B (2020) Neurologic Manifestations of Hospitalized Patients With Coronavirus Disease 2019 in Wuhan, China. JAMA Neurol 77:683. [PubMed: 32275288]

Marcinkiewcz CA (2015) Serotonergic Systems in the Pathophysiology of Ethanol Dependence: Relevance to Clinical Alcoholism. ACS Chem Neurosci.

Marcinkiewcz CA, Dorrier CE, Lopez AJ, Kash TL (2014) Ethanol induced adaptations in 5-HT2c receptor signaling in the bed nucleus of the stria terminalis: Implications for anxiety during ethanol withdrawal. Neuropharmacology 89C:157–167.

Marcinkiewcz CA, Lowery-Gionta EG, Kash TL (2016a) Serotonin's Complex Role in Alcoholism: Implications for Treatment and Future Research. Alcohol Clin Exp Res 40:1192–1201. [PubMed: 27161942]

Maul B, Krause W, Pankow K, Becker M, Gembardt F, Alenina N, Walther T, Bader M, Siems W (2005) Central angiotensin II controls alcohol consumption via its AT1 receptor. The FASEB Journal 19:1474–1481. [PubMed: 16126915]

McCray PB, Pewe L, Wohlford-Lenane C, Hickey M, Manzel L, Shi L, Netland J, Jia HP, Halabi C, Sigmund CD, Meyerholz DK, Kirby P, Look DC, Perlman S (2007) Lethal Infection of K18-hACE2 Mice Infected with Severe Acute Respiratory Syndrome Coronavirus . J Virol.

Meyerholz DK, Edsen-Moore M, McGill J, Coleman RA, Cook RT, Legge KL (2008) Chronic Alcohol Consumption Increases the Severity of Murine Influenza Virus Infections. The Journal of Immunology.

Muhammad JS, Siddiqui R, Khan NA (2021) COVID-19: Is There a Link between Alcohol Abuse and SARS-CoV-2-Induced Severe Neurological Manifestations? ACS Pharmacol Transl Sci.

Netland J, Meyerholz DK, Moore S, Cassell M, Perlman S (2008) Severe Acute Respiratory Syndrome Coronavirus Infection Causes Neuronal Death in the Absence of Encephalitis in Mice Transgenic for Human ACE2. J Virol.

Okuno F, Arai M, Ishii H, Shigeta Y, Ebihara Y, Takagi S, Tsuchiya M (1986) Mild but prolonged elevation of serum angiotensin converting enzyme (ACE) activity in alcoholics. Alcohol.

Pang X, Cui Y, Zhu Y (2020) Recombinant human ACE2: potential therapeutics of SARS-CoV-2 infection and its complication. Acta Pharmacol Sin 41:1255–1257. [PubMed: 32581256]

Papp RS (2014) Brainstem projections of neurons located in various subdivisions of the dorsolateral hypothalamic area – an anterograde tract-tracing study. Front Neuroanat 8.

Piras IS, Huentelman MJ, Walker JE, Arce R, Glass MJ, Vargas D, Sue LI, Intorcia AJ, Nelson CM, Suszczewicz KE, Borja CL, Desforges M, Deture M, Dickson DW, Beach TG, Serrano GE (2021) Olfactory Bulb and Amygdala Gene Expression Changes in Subjects Dying with COVID-19. medRxiv.

Pitel AL, Segobin SH, Ritz L, Eustache F, Beaunieux H (2015) Thalamic abnormalities are a cardinal feature of alcohol-related brain dysfunction. Neurosci Biobehav Rev 54:38–45. [PubMed: 25108034]

Qiao J, Li W, Bao J, Peng Q, Wen D, Wang J, Sun B (2020) The expression of SARS-CoV-2 receptor ACE2 and CD147, and protease TMPRSS2 in human and mouse brain cells and mouse brain tissues. Biochem Biophys Res Commun 533:867–871. [PubMed: 33008593]

Quijano A, Diaz-Ruiz C, Lopez-Lopez A, Villar-Cheda B, Muñoz A, Rodriguez-Perez AI, Labandeira-Garcia JL (2022) Angiotensin Type-1 Receptor Inhibition Reduces NLRP3 Inflammasome Upregulation Induced by Aging and Neurodegeneration in the Substantia Nigra of Male Rodents and Primary Mesencephalic Cultures. Antioxidants 11:329. [PubMed: 35204211]

Rachdaoui N, Sarkar DK (2017) Pathophysiology of the Effects of Alcohol Abuse on the Endocrine System. Alcohol Res 38:255–276. [PubMed: 28988577]

Rahman MM, Hasan M, Ahmed A (2021) Potential detrimental role of soluble ACE2 in severe COVID-19 comorbid patients. Rev Med Virol 31:1–12.

Reeh H, Rudolph N, Billing U, Christen H, Streif S, Bullinger E, Schliemann-Bullinger M, Findeisen R, Schaper F, Huber HJ, Dittrich A (2019) Response to IL-6 trans- and IL-6 classic signalling is determined by the ratio of the IL-6 receptor α to gp130 expression: fusing experimental insights and dynamic modelling. Cell Communication and Signaling 17:46. [PubMed: 31101051]

Roberto M, Kirson D, Khom S (2021) The Role of the Central Amygdala in Alcohol Dependence. Cold Spring Harb Perspect Med 11:a039339. [PubMed: 31988201]

Sagarkar S, Choudhary AG, Balasubramanian N, Awathale SN, Somalwar AR, Pawar N, Kokare DM, Subhedar NK, Sakharkar AJ (2021) LSD1-BDNF activity in lateral hypothalamus-medial forebrain bundle area is essential for reward seeking behavior. Prog Neurobiol 202:102048. [PubMed: 33798614]

Samuels E, Szabadi E (2008) Functional Neuroanatomy of the Noradrenergic Locus Coeruleus: Its Roles in the Regulation of Arousal and Autonomic Function Part I: Principles of Functional Organisation. Curr Neuropharmacol 6:235–253. [PubMed: 19506723]

Saurabh S, Verma MK, Gautam V, Kumar N, Jain V, Goel AD, Gupta MK, Sharma PP, Bhardwaj P, Singh K, Nag VL, Garg MK, Misra S (2021) Tobacco, alcohol use and other risk factors for developing symptomatic COVID-19 vs asymptomatic SARS-CoV-2 infection: A case-control study from western Rajasthan, India. Trans R Soc Trop Med Hyg.

Schmittgen TD, Livak KJ (2008) Analyzing real-time PCR data by the comparative CT method. Nat Protoc 3:1101–1108. [PubMed: 18546601]

Selvakumar GP, Ahmed ME, Thangavel R, Kempuraj D, Dubova I, Raikwar SP, Zaheer S, Iyer SS, Zaheer A (2020) A role for glia maturation factor dependent activation of mast cells and microglia in MPTP induced dopamine loss and behavioural deficits in mice. Brain Behav Immun.

Siddiqui R (2021) SARS-CoV-2 invasion of the central nervous : a brief review. Hosp Pract 00:1–7.

Smith HR, Leibold NK, Rappoport DA, Ginapp CM, Purnell BS, Bode NM, Alberico SL, Kim Y-C, Audero E, Gross CT, Buchanan GF (2018) Dorsal Raphe Serotonin Neurons Mediate CO 2 -Induced Arousal from Sleep. The Journal of Neuroscience 38:1915–1925. [PubMed: 29378860]

Song E, Zhang C, Israelow B, Lu-Culligan A, Prado AV, Skriabine S, Lu P, Weizman O el, Liu F, Dai Y, Szigeti-Buck K, Yasumoto Y, Wang G, Castaldi C, Heltke J, Ng E, Wheeler J, Alfajaro MM, Levavasseur E, Fontes B, Ravindra NG, van Dijk D, Mane S, Gunel M, Ring A, Jaffar Kazmi SA, Zhang K, Wilen CB, Horvath TL, Plu I, Haik S, Thomas JL, Louvi A, Farhadian SF, Huttner A,

Seilhean D, Renier N, Bilguvar K, Iwasaki A (2021) Neuroinvasion of SARS-CoV-2 in human and mouse brain. Journal of Experimental Medicine.

Tang AT, Buchholz DW, Szigety KM, Imbhiaka B, Gao S, Frankfurter M, Wang M, Yang J, Hewins P, Mericko-Ishizuka P, Adrian Leu N, Sterling S, Monreal IA, Sahler J, August A, Zhu X, Jurado KA, Xu M, Morrisey EE, Millar SE, Aguilar HC, Kahn ML (2021) SARS-CoV-2 infection of olfactory epithelial cells and neurons drives acute lung injury and lethal COVID-19 in mice. bioRxiv.

Tang T, Bidon M, Jaimes JA, Whittaker GR, Daniel S (2020) Coronavirus membrane fusion mechanism offers a potential target for antiviral development. Antiviral Res 178:104792. [PubMed: 32272173]

Testino G (2020) Are Patients with Alcohol Use Disorders at Increased Risk for Covid-19 Infection. Alcohol and Alcoholism.

Tran S, Kuruppu S, Rajapakse NW (2022) Chronic Renin-Angiotensin System Activation Induced Neuroinflammation: Common Mechanisms Underlying Hypertension and Dementia? Journal of Alzheimer's Disease 85:943–955.

Ueha R, Kondo K, Kagoya R, Shichino S, Ueha S, Yamasoba T (2020) ACE2, TMPRSS2, and Furin expression in the nose and olfactory bulb in mice and human. Rhinology journal 0–0.

Underwood MD, Mann JJ, Arango V (2007) Morphometry of Dorsal Raphe Nucleus Serotonergic Neurons in Alcoholism. Alcohol Clin Exp Res 31:837–845. [PubMed: 17378916]

Wang L, de Kloet AD, Pati D, Hiller H, Smith JA, Pioquinto DJ, Ludin JA, Oh SP, Katovich MJ, Frazier CJ, Raizada MK, Krause EG (2016) Increasing brain angiotensin converting enzyme 2 activity decreases anxiety-like behavior in male mice by activating central Mas receptors. Neuropharmacology 105:114–123. [PubMed: 26767952]

Zipeto D, Palmeira J da F, Argañaraz GA, Argañaraz ER (2020) ACE2/ADAM17/TMPRSS2 Interplay May Be the Main Risk Factor for COVID-19. Front Immunol.

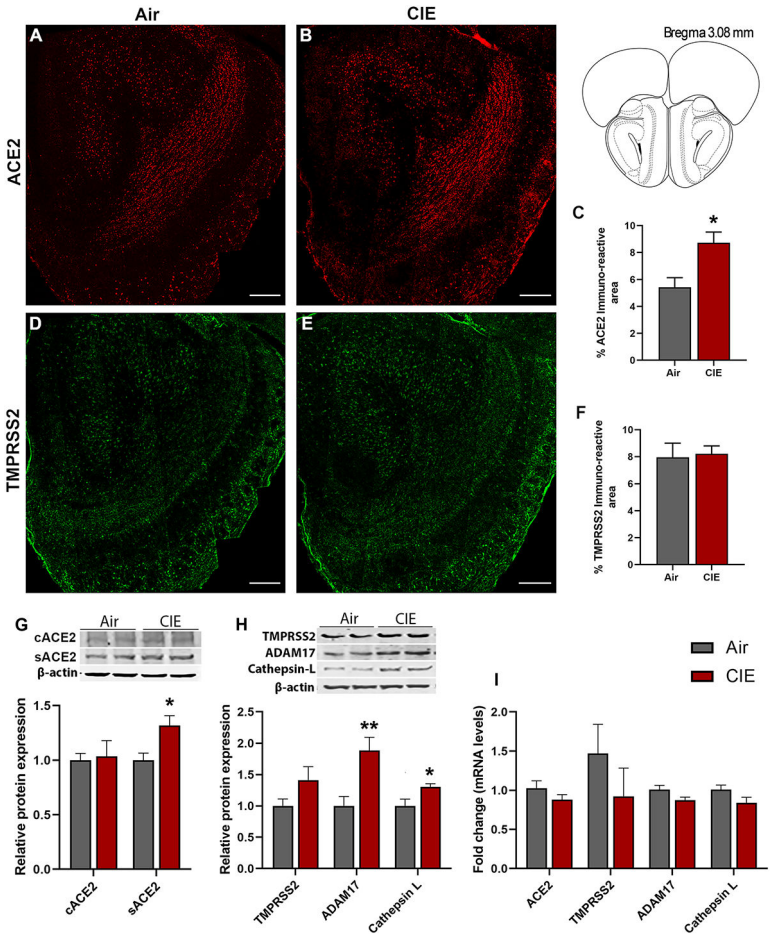

Figure 1: Effect of chronic intermittent ethanol (CIE) exposure on the ACE2, TMPRSS2, ADAM17, and Cathepsin L expression in the olfactory bulb (OB).

(A-B) Representative confocal images of ACE2 positive cells in OB of air control and CIE mice. Scale bar = 200 μm **(C)** Histogram represents the % ACE2 immunoreactive area in OB. **(D-E)** Representative confocal images of TMPRSS2 in OB of air control and CIE mice. Scale bar = 200 μm. **(F)** Histogram showing the % TMPRSS2 immunoreactive area in OB. **(G)** Representative Western blot (WB) and histogram showing the cACE2 and sACE2 protein levels in the OB. **(H)** Representative WB and histogram showing the TMPRSS2, ADAM17, and Cathepsin L protein levels in the OB. **(I)** Histogram showing the ACE2, TMPRSS2, ADAM17, and Cathepsin L mRNA levels in the OB. Values (n = 4 - 5/group for IF and n = 7-8/group for WB and RT-qPCR) are represented as means (±SEM) and the data was analyzed by unpaired student's t-test with Welch's correction (*p < 0.05, **p < 0.01, versus air control).

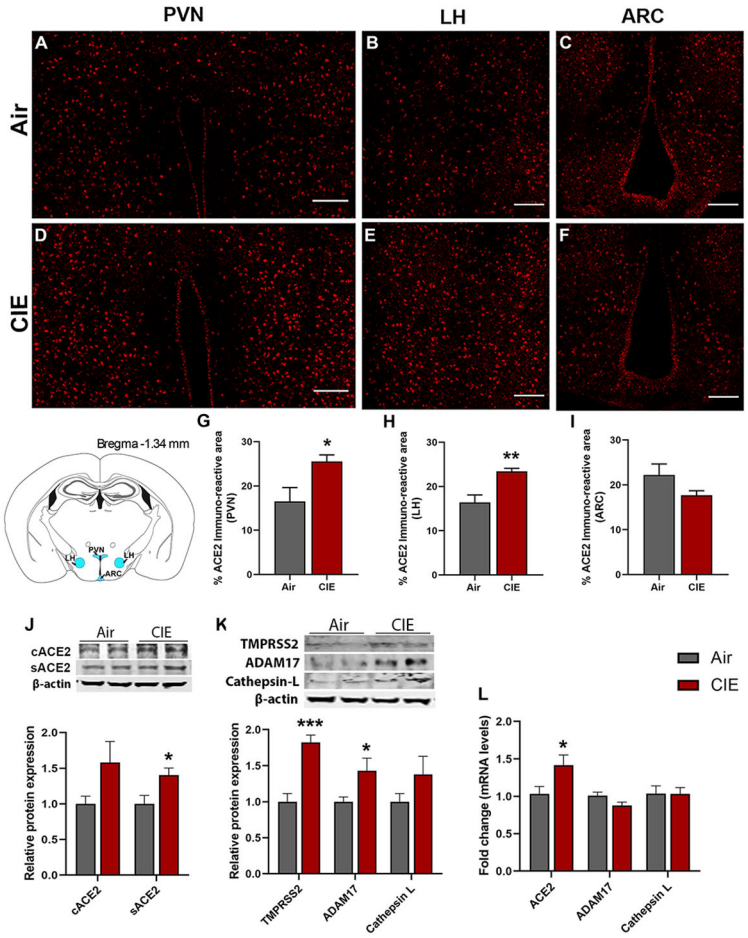

Figure 2: Effect of chronic intermittent ethanol (CIE) exposure on the ACE2, TMPRSS2, ADAM17, and Cathepsin L expression in hypothalamic nuclei.

Representative confocal images of ACE2 positive cells in **(A,D)** PVN, **(B,E)** LH and **(C,F)** ARC of air control and CIE mice. Scale bar = 100 μm. **(G-I)** Histograms showing the % ACE2 immunoreactive area in PVN, LH, and ARC. **(J)** Representative Western blot (WB) and histogram showing the cACE2 and sACE2 protein levels in the hypothalamus. **(K)** Representative WB and histogram showing the TMPRSS2, ADAM17, and Cathepsin L protein levels in the hypothalamus. **(L)** Histogram showing the ACE2, ADAM17, and Cathepsin L mRNA levels in the hypothalamus. Values (n = 4 - 5/group for IF and n = 7-8/group for WB and RT-qPCR) are represented as means (±SEM) and the data was analyzed by unpaired student's t-test with Welch's correction (*p < 0.05, **p < 0.01, ***p < 0.001 versus air control).

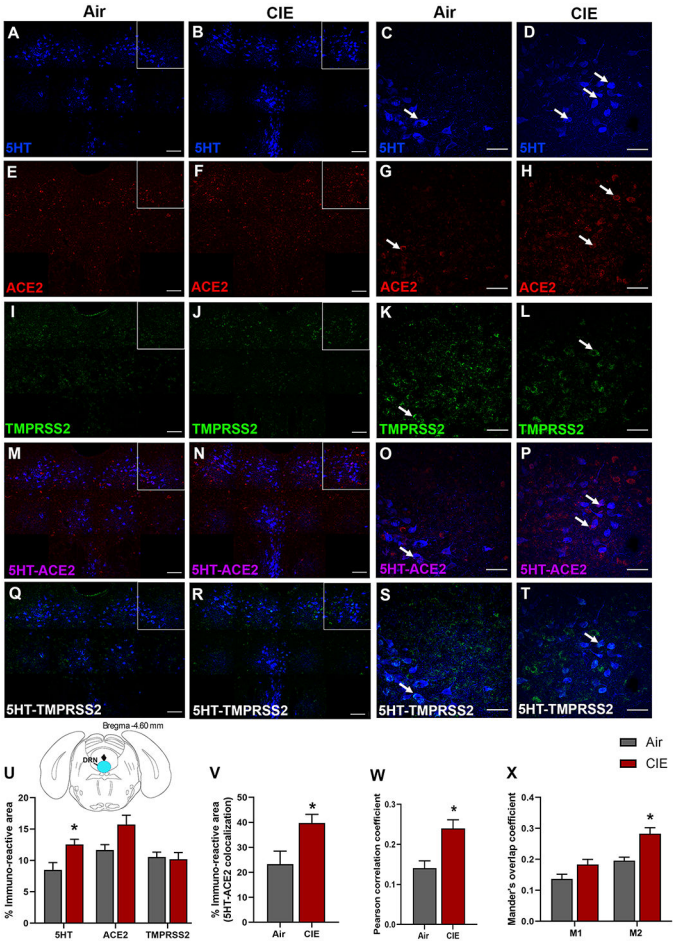

Figure 3: Effect of chronic intermittent ethanol (CIE) exposure on the 5HT, ACE2, and TMPRSS2 immunoreactivity in dorsal raphe nucleus (DRN).

Representative confocal images showing **(A-B)** 5-HT in the DRN (blue; scale bar = 100 μm) and **(C-D)** a single tile image (scale bar = 50 μm) from the boxed area of air control and CIE mice. **(E-F)** Representative images of ACE2 (red; scale bar = 100 μm) in the DRN and **(G-H)** a single tile image (scale bar = 50 μm) from the boxed area in air control and CIE mice. **(I-J)** TMPRSS2 (green; scale bar = 100 μm) in the DRN and **(K-L)** a single tile image (scale bar = 50 μm) from the boxed area in air control and CIE mice. **(M-N)** 5HT-ACE2 (magenta) colocalization in the DRN and **(O-P)** a single tile image from the boxed area in air control and CIE mice. **(Q-R)** 5HT-TMPRSS2 (white) positive neurons in the DRN and **(S-T)** a single tile image from the boxed area of air control and CIE mice. Histogram showing **(U)** % immunoreactive area for 5HT, ACE2, and TMPRSS2, **(V)** % immunoreactive area for 5HT-ACE2 positive neurons, **(W)** Pearson correlation coefficient for 5HT-ACE2 colocalization **(X)** Mander's overlap coefficient for 5HT-ACE2 colocalization in DRN. Values (n = 4 - 5/group) are represented as means (±SEM) and the data was analyzed by unpaired student's t-test with Welch's correction (*$p < 0.05$ versus air control).

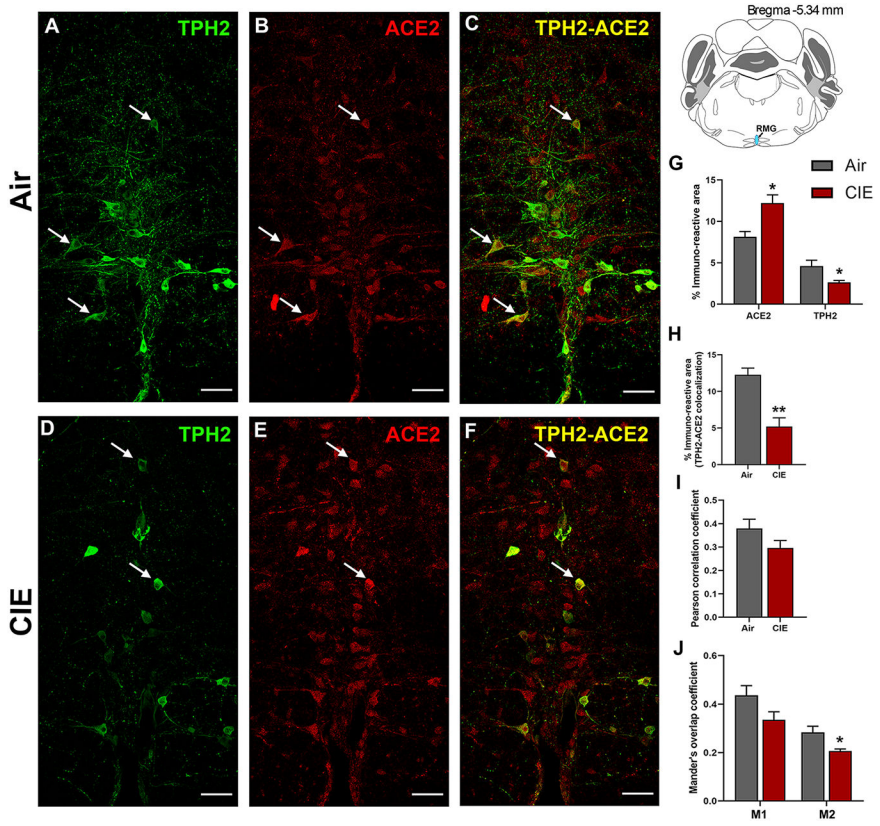

Figure 4: Effect of chronic intermittent ethanol (CIE) exposure on the TPH2 and ACE2 immunoreactivity in raphe magnus (RMG).

Representative confocal images showing **(A and D)** TPH2 (green) **(B and E)** ACE2 (red) **(C and F)** TPH2-ACE2 (yellow) positive neurons in RMG of air and CIE mice. Scale bar = 50 μm. Graph showing **(G)** % immunoreactive area for ACE2 and TPH2, **(H)** % immunoreactive area for TPH2-ACE2 positive neurons, **(I)** Pearson correlation coefficient for TPH2-ACE2 colocalization **(J)** Mander's overlap coefficient for TPH2-ACE2 colocalization in RMG. Values (n = 4 - 5/group) are represented as means (±SEM) and the data was analyzed by unpaired student's t-test with Welch's correction (*$p < 0.05$, **$p < 0.01$ versus air control).

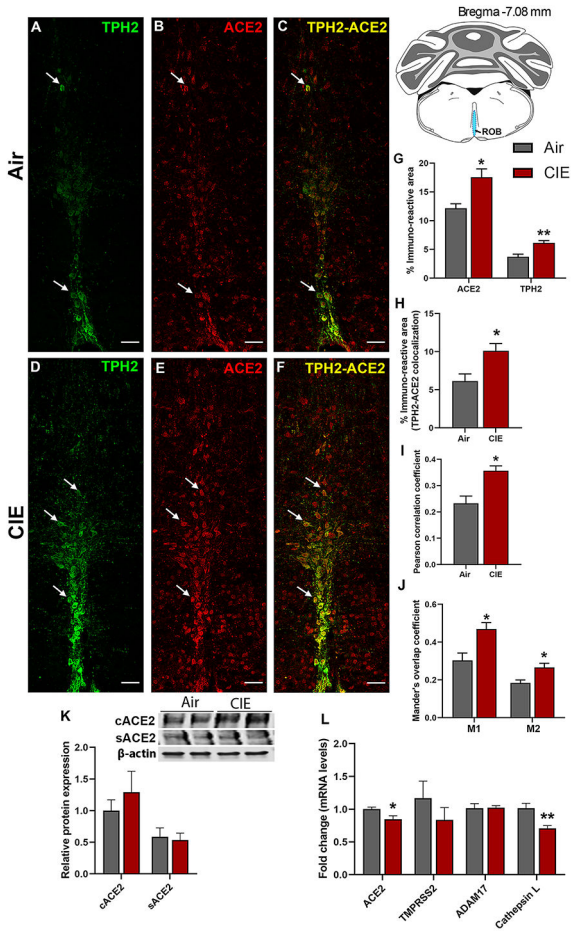

Figure 5: Effect of chronic intermittent ethanol (CIE) exposure on the ACE2-TPH2 immunoreactivity in raphe obscurus (ROB) and ADAM17, TMPRSS2, and Cathepsin L expression in medullary raphe.

Representative confocal images showing **(A and D)** TPH2 (green) **(B and E)** ACE2 (red) **(C and F)** TPH2-ACE2 (yellow) positive neurons in ROB of air control and CIE mice. Scale bar = 50 μm. Graph showing **(G)** % immunoreactive area for ACE2 and TPH2, **(H)** % immunoreactive area for TPH2-ACE2 positive neurons, **(I)** Pearson correlation coefficient for TPH2-ACE2 colocalization **(J)** Mander's overlap coefficient for TPH2-ACE2 colocalization in ROB. **(K)** Representative Western blot (WB) and histogram showing the cACE2 and sACE2 protein levels in the medullary raphe. **(L)** Histogram showing the ACE2, TMPRSS2, ADAM17, and Cathepsin L mRNA levels in the medullary raphe. Values (n = 4 - 5/group for IF and n = 7-8/group for WB and RT-qPCR) are represented as means (±SEM) and the data was analyzed by unpaired student's t-test with Welch's correction (*$p < 0.05$, **$p < 0.01$ versus air control).

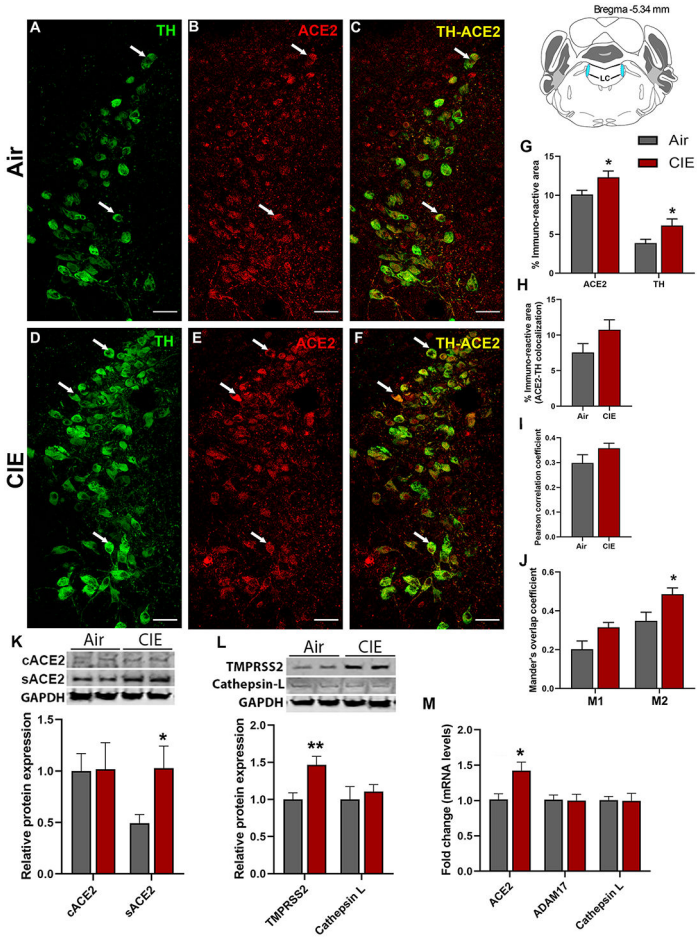

Figure 6: Effect of chronic intermittent ethanol (CIE) exposure on the ACE2, TH, ADAM17, TMPRSS2, and Cathepsin L expression in locus coeruleus (LC).

Representative confocal images showing **(A and D)** TH (green) **(B and E)** ACE2 (red) **(C and F)** TH-ACE2 (yellow) positive neurons in LC of air and CIE mice. Scale bar = 50 μm. Graph showing **(G)** % immunoreactive area for ACE2 and TH, **(H)** % immunoreactive area for TH-ACE2 positive neurons, **(I)** Pearson correlation coefficient for TH-ACE2 colocalization **(J)** Mander's overlap coefficient for TH-ACE2 colocalization in LC. **(K)** Representative Western blot (WB) and histogram showing the cACE2 and sACE2 protein levels in the LC. **(L)** Representative WB and histogram showing the TMPRSS2, and Cathepsin L protein levels in the LC. **(M)** Histogram showing the ACE2, ADAM17, and Cathepsin L mRNA levels in the LC. Values (n = 4 - 5/group for IF and n = 7-8/group for WB and RT-qPCR) are represented as means (±SEM) and the data was analyzed by unpaired student's t-test with Welch's correction (*p < 0.05, **p < 0.01 versus air control).

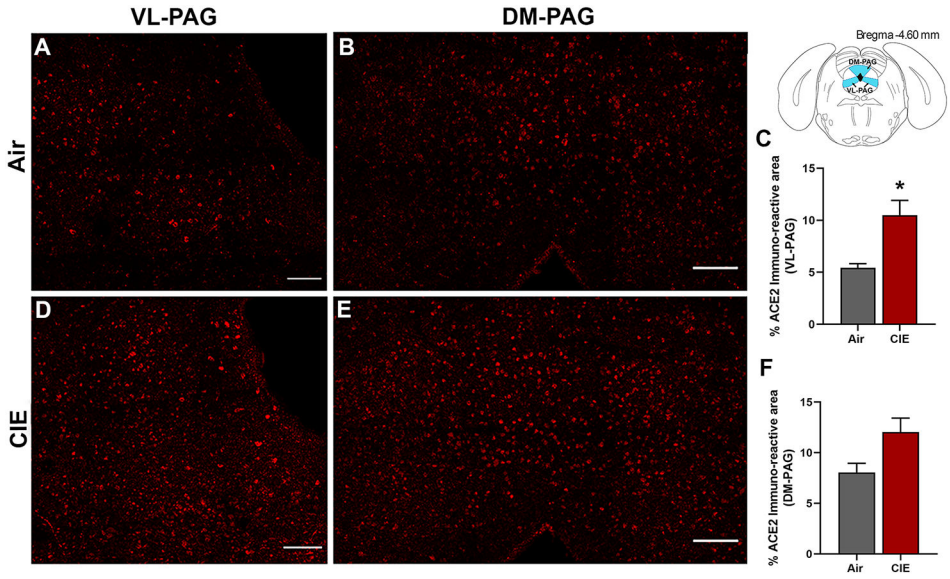

Figure 7: Effect of chronic intermittent ethanol (CIE) exposure on the ACE2 immunoreactivity in the ventrolateral and dorsomedial periaqueductal gray (VL-PAG, DM-PAG).

Representative confocal images showing ACE2 positive cells in **(A, D)** VL-PAG and **(B, E)** DM-PAG of air and CIE mice. Scale bar = 100 μm. **(C)** Histogram showing the % ACE2 immunoreactive area in VL-PAG and **(F)** DM-PAG. Values (n = 4 - 5/group) are represented as means (±SEM) and the data was analyzed by unpaired student's t-test with Welch's correction (*$p < 0.05$ versus air control).

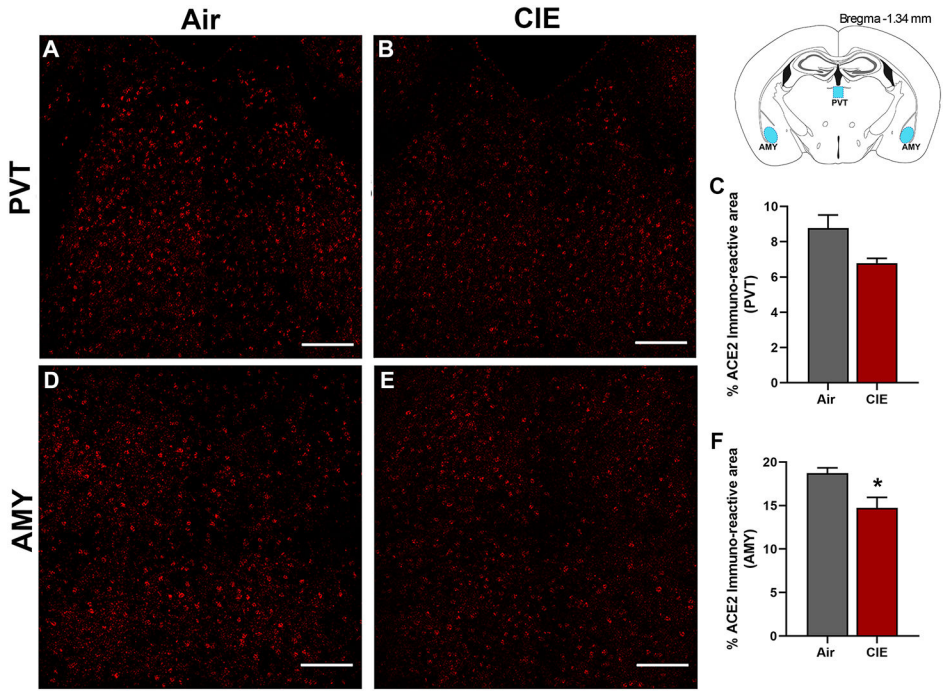

Figure 8: Effect of chronic intermittent ethanol (CIE) exposure on the ACE2 immunoreactivity in the paraventricular thalamic nucleus (PVT) and amygdala (AMY).

Representative confocal images showing ACE2 positive cells in **(A-B)** PVT **(D-E)** AMY of air and CIE mice. Scale bar = 100 μm. Histogram showing the % ACE2 immunoreactive area in **(C)** PVT **(F)** in AMY. Values (n = 4 - 5/group) are represented as means (±SEM) and the data was analyzed by unpaired student's t-test with Welch's correction (*$p < 0.05$ versus air control).

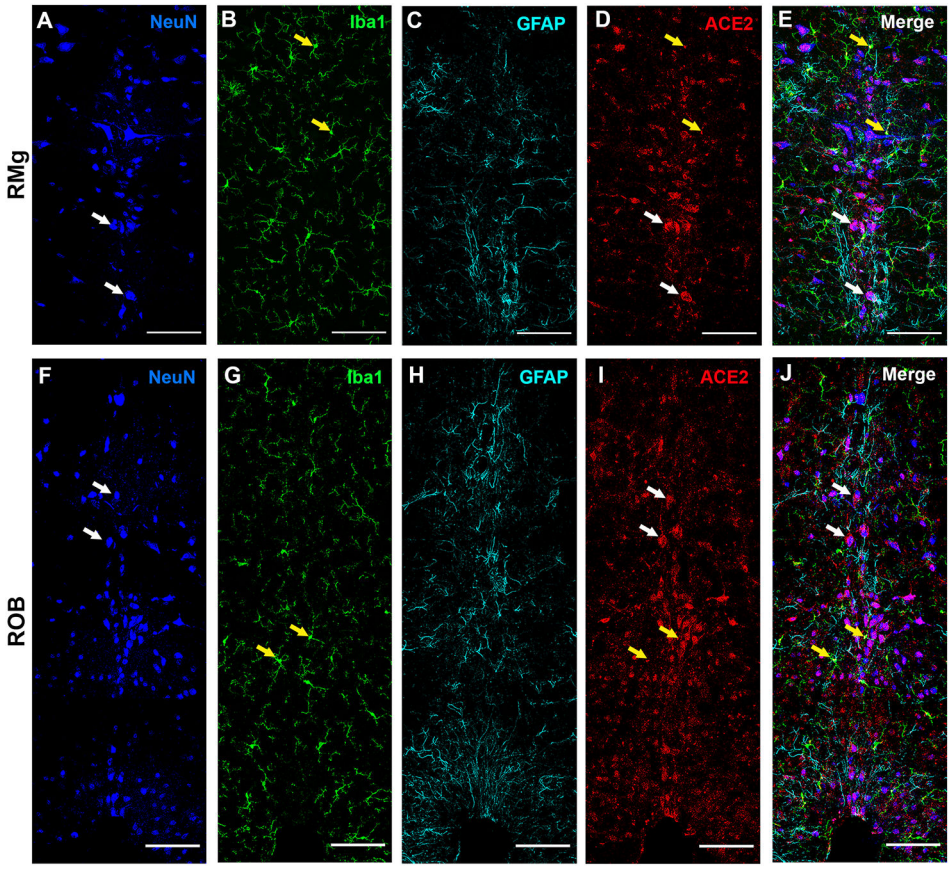

Figure 9: ACE2 distribution in neurons, microglia, and astrocyte in medullary raphe nuclei.

The raphe magnus (RMG), and raphe obscurus (ROB) were stained for neuronal marker NeuN **(panel A, F)**; microglia marker Iba1 **(panel B, G)**; astrocyte marker GFAP **(panel C, H)** and ACE2 **(panel D, I)**. Panel E shows the merged image of the RMG stained with all the markers **(panels A-C)** with ACE2 **(panel D)**. Panel J shows the merged image of the ROB stained with all the markers **(panels F-H)** with ACE2 **(panel I)**. Yellow arrows indicate the colocalization of ACE2 and Iba1 (yellow in the merge panels) and white arrows indicate the colocalization of ACE2 and NeuN (magenta in the merge panels). Scale bar = 100um.

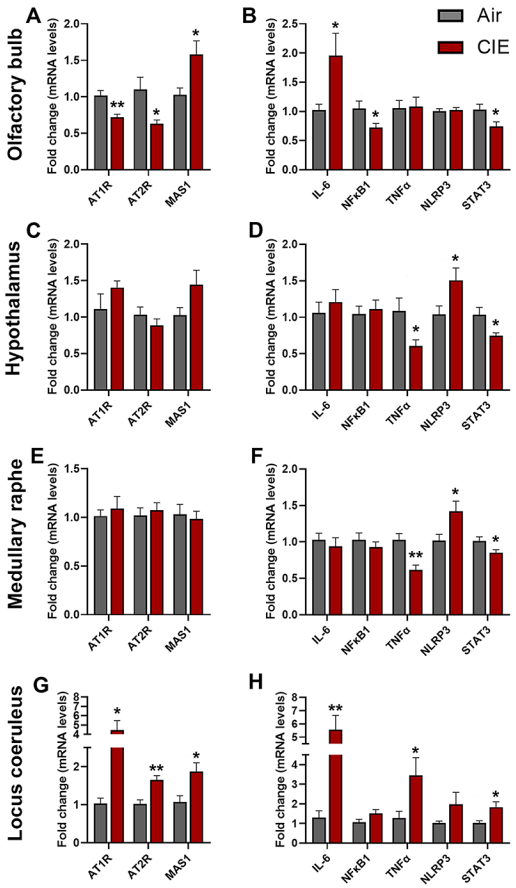

Figure 10: Effect of chronic intermittent ethanol (CIE) exposure on mRNA expression of the RAS pathway and pro-inflammatory receptors.

RAS pathway receptor (AT1R, AT2R, MAS1) mRNA expression in **(A)** Olfactory bulb **(C)** Hypothalamus **(E)** Medullary raphe **(G)** Locus coeruleus. Pro-inflammatory marker (*Il-6, Nfkb1, Tnfα, Nlrp3, Stat3*) mRNA expression in **(B)** Olfactory bulb **(D)** Hypothalamus **(F)** Medullary raphe **(H)** Locus coeruleus. Values (n = 7 - 8/group) are represented as means (±SEM) and the data was analyzed by multiple unpaired student's t-test (*p < 0.05, **p < 0.01, versus air control).

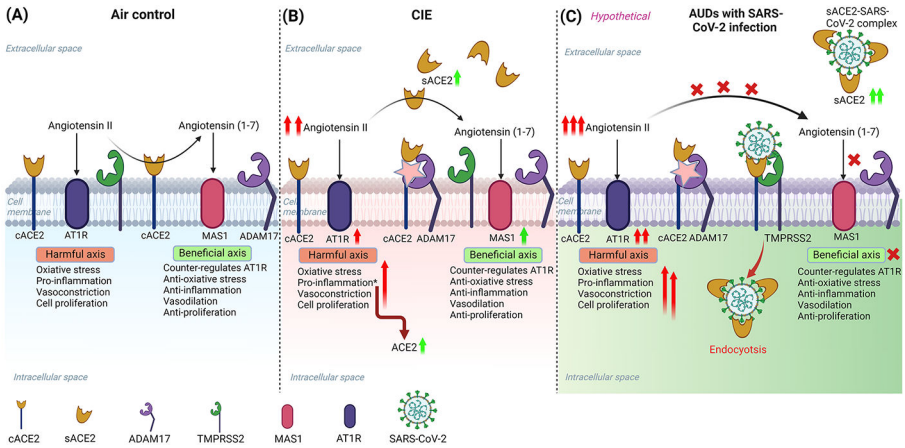

Figure 11: Schematic overview of the possible mechanism for increased susceptibility to SARS-CoV-2 infection in alcohol use disorder patients.

(A) *Baseline mechanism:* Angiotensin-converting enzyme 2 (ACE2) is a key regulator of the Renin-angiotensin system (RAS) that controls the hyperactivation of the Angiotensin II-AT1R pathway by converting Angiotensin II to Angiotensin (1-7) and activating MAS1 receptor-mediated pathway. **(B)** *RAS perturbation by ethanol intake:* After ethanol intoxication, the homeostatic balance of the RAS in the CNS is disturbed due to higher Angiotensin II levels, and the hyperactivation of the Angiotensin II-AT1R axis leads to neuroinflammation. A soluble form of ACE2 (sACE2) levels are increased after ethanol due to higher levels of ADAM17 (ACE2 sheddase) in the CNS, to cope with Angiotensin II triggered inflammation. **(C)** *A hypothetical model explaining the susceptibility of AUDs to increased risk for SARS-CoV-2 infection:* Ethanol exacerbates the levels of sACE2 to compensate for the harmful effects of Angiotensin II in the CNS. However, after infection with SARS-CoV-2, the virus hijacks the sACE2 and gets internalized into the cell by endocytosis, thereby reducing the circulating sACE2 and perturbing the homeostasis in the RAS leading to neuroinflammation and other pathological complications. The illustration was created in BioRender (BioRender.com).

Table 1:

List of primers used for quantitating mRNA expression using RT-qPCR

Gene Name	Forward/Reverse (5'-3')	Sequence
β-actin	Forward	CCAGCCTTCCTTCTTGGGTA
	Reverse	GAGGTCTTTACGGATGTCAACG
Ace2	Forward	TGGGACACGGAGACTTCAGA
	Reverse	TGGCTCCGTTTCTTAGCAGG
Tmprss2	Forward	TGAAACGCCAGAGCAGGATT
	Reverse	AAATGCCGTCCAGTACCTCG
Adam17	Forward	GAAGACCCCAGCACAGACTC
	Reverse	CCTTTTCGCTCCTGGTGACT
Cathepsin L	Forward	GTCTTGTTGGGCGTTTAGCG
	Reverse	TGAGCGTGAGAACAGTCCAC
At1r	Forward	ACAACTGCCTGAACCCTCTG
	Reverse	ACCTCAGAACAAGACGCAGG
At2r	Forward	TTTGTTCTGGGCTTCGTCCC
	Reverse	CTTGCCATTTGCTGGGTCTG
Mas1	Forward	ACCTCCAGCAGAAATGCCTC
	Reverse	TCCCATTCTCCACAAAGCCC
Il-6	Forward	GAGACTTCCATCCAGTTGCCT
	Reverse	TCCTCTGTGAAGTCTCCTCTCC
Nfκb1	Forward	ACTGTCTGCCTCTCTCGTCT
	Reverse	CCGTGGGGCATTTTGTTCAG
Tnfα	Forward	CGGGCAGGTCTACTTTGGAG
	Reverse	ACCCTGAGCCATAATCCCCT
Nlrp3	Forward	CAAGGCTGCTATCTGGAGGAA
	Reverse	TTCTCGGGCGGGTAATCTTC
Stat3	Forward	TTGTCGGTTGGAGGTGTGAG
	Reverse	AAGTGGGAAAGGAAGGCAGG

Table 2:

Details of the antibodies used in the western blot experiments

Antibodies	Use	Catalog details	Company	Dilution
ACE2	Primary	AF933	Novus Biologicals	1:250
TMPRSS2	Primary	sc-515727	Santa Cruz Biotechnology	1:1000
Cathepsin-L	Primary	sc-390385	Santa Cruz Biotechnology	1:1000
ADAM17	Primary	NBP2-15281	Novus Biologicals	1:1000
β-actin	Primary	sc-47778	Santa Cruz Biotechnology	1:8000
GAPDH	Primary	G9545	Millipore Sigma	1:8000
IRDye 800CW anti-Mouse	Secondary	926-32212	LI-COR	1:6000
IRDye 680RD anti-Goat	Secondary	926-68074	LI-COR	1:6000
IRDye 680RD anti-Rabbit	Secondary	926-68073	LI-COR	1:6000

Table 3:

Details of the antibodies used in immunofluorescence experiments

Antibodies	Use	Catalog details	Company	Dilution
ACE2	Primary	AF933	Novus Biologicals	1:250
TMPRSS2	Primary	sc-515727	Santacruz	1:300
TPH2	Primary	NB100-7455	Novus Biologicals	1:1000
5HT	Primary	20080	Immunostar	1:4000
TH	Primary	MAB-318	Millipore	1:200
NeuN	Primary	ABN90	Millipore	1:2000
GFAP	Primary	ab4674	Abcam	1:5000
Iba-1	Primary	ab178846	Abcam	1:1000
Donkey Anti-Goat	Secondary	705-165-147	Jackson Immunoresearch laboratories	1:800
Donkey Anti-Mouse	Secondary	715-545-150	Jackson Immunoresearch laboratories	1:800
Donkey Anti-Rabbit	Secondary	A31573	Invitrogen	1:800
Donkey Anti-Rabbit	Secondary	711-475-152	Jackson Immunoresearch laboratories	1:800
Donkey Anti-Guinea Pig	Secondary	706-475-148	Jackson Immunoresearch laboratories	1:800
Donkey Anti-Chicken	Secondary	703-605-155	Jackson Immunoresearch laboratories	1:800